

The Effect of Airway Wall Motion on Surfactant Delivery

D. Halpern

Department of Mathematics,
University of Alabama,
Tuscaloosa, AL 35487

J. L. Bull

J. B. Grotberg

Biomedical Engineering Department,
The University of Michigan,
Ann Arbor, MI 48109

Soluble surfactant and airway surface liquid transport are examined using a mathematical model of Marangoni flows which accounts for airway branching and for cyclic airway stretching. Both radial and longitudinal wall strains are considered. The model allows for variation of the amplitude and frequency of the motion, as may occur under a variety of ventilatory situations occurring during surfactant replacement therapy. The soluble surfactant dynamics of the thin fluid film are modeled by linear sorption. The delivery of surfactants into the lung is handled by setting the proximal boundary condition to a higher concentration compared to the distal boundary condition. Starting with a steady-state, nonuniform, surfactant distribution, we find that transport of surfactant into the lung is enhanced for increasing strain amplitudes. However, for fixed amplitude, increasing frequency has a smaller effect. At small strain amplitudes, increasing frequency enhances transport, but at large strain amplitudes, increasing cycling frequency has the opposite effect. [DOI: 10.1115/1.1784475]

Introduction

The transport of surfactant and airway surface liquid within the lung is important in many clinical applications ranging from surfactant replacement therapy (SRT) [1–4] to clearance of surfactant and liquid from the lung. Applications of liquid delivery without surfactants, for example, include liquid ventilation [5–9]. When a liquid is instilled into the trachea at a fast enough rate, it forms a plug [10]. In the larger airways, air-driven plug flow and gravity-driven flow dominate the transport mechanisms [11,12]. As the liquid thins distally, Marangoni flows become the prevalent transport mechanisms in the smaller airways. The presence of pre-existing surfactant on the air-liquid interface, which may be from a previous SRT dose or produced by the alveolar type II cells, can impede the Marangoni flow since it lowers the surface tension gradient driving the flow of subsequent doses [13].

Theoretical models of flows within thin viscous layers due to surfactant induced Marangoni stresses are based on lubrication theory, from which coupled evolution equations for film thickness and surfactant surface concentration are derived [13–23]. The transient spreading of an insoluble surfactant on an otherwise clean interface results in a wave which travels in the direction of higher surface tension (lower surfactant concentration). If surface diffusion and gravity are negligible, the wave behaves like a kinematic shock wave and there is a large change in film height and surface tension over a very short distance [24]. The film thickens to twice its undisturbed height at the traveling shock. The film thins significantly behind the shock, which may lead to rupture [14,16,21–23]. Film rupture has been observed in experiments [21–23,25–27], and is an undesired result for SRT, as it causes the surfactant to stop spreading. The effects of solubility on surfactant spreading on a clean interface have been studied by Halpern & Grotberg [28,29] and Jensen & Grotberg [28,29] who found that wall uptake of surfactant can result in reversal of the propagation of the leading edge of the new surfactant front.

The effect of pre-existing surfactant has also been investigated [13,21,22]. Although the spreading rate of the new surfactant is slowed by the presence of pre-existing surfactant, a surface-compression disturbance propagates through the pre-existing surfactant at a faster speed than the leading edge of the new surfactant front. Whereas higher pre-existing surfactant concentrations cause the leading edge of the new surfactant front to travel slower,

they result in faster propagation of the compression disturbance. The propagation speed of the compression disturbance is related to an effective diffusivity that is inversely proportional to the pre-existing surfactant surface concentration [21]. The compression disturbance increases the local surface concentration of the pre-existing surfactant before the new surfactant arrives.

Once the initial wave of spreading has occurred, a steady state distribution of surfactant and film thickness is established, as studied in [11] for pulmonary applications. Other studies of steady surfactant transport along thin films include [30,31], the latter being applied to surfactant clearance from the lung. The steady motion of a liquid film due to surface tension gradients has been considered by Yih [30] who found that a boundary layer whose thickness is the order of the film thickness exists near any vertical boundary. Davis et al. [31] solved for steady state film thickness and surface tension profiles for insoluble surfactant on a film coating a tube.

Espinosa [32] examined effects of longitudinal stretching on liquid transport related to clearance. An initially uniform surface concentration of surfactant on a thin liquid film, constrained to no flux at both ends or one end, was subjected to a time-periodic, spatially-linear strain for one cycle. Linear strain helps to account for the axial variation in airway elastic properties, the proximal end (trachea) being stiffer than the distal end (acinus). Calculations of the mid-axial liquid flow were used to estimate the effect of the oscillations on liquid transport. Their model allowed for squeeze-out of surfactant from the interface to the bulk, while assuming the bulk concentration of surfactant to be uniform and constant. They found that liquid transport toward the stiffer end of the wall experiences an optimal cycling period for which the volume of liquid on the distal half of the membrane is maximal. Smaller or larger periods reduce the transport. Also, as they increased longitudinal wall strain amplitude, the liquid transport diminished and, in some cases, reversed direction toward the less-stiff end.

In the present work, we consider a thin film supported by a stretchable membrane and examine the effects of in-plane wall oscillations on surfactant transport, in order to gain a better understanding of the effect of breathing on SRT. The wall model is a branching network of tubes whose effect is approximated by considering the perimeter to vary with position along the airway tree. This branching is a significant feature of lung anatomy. Breathing motions are modeled by cycling the radius and length of each individual airway. The cycling uses a uniform axial strain. A steady-state surfactant concentration and liquid film thickness pro-

Contributed by the Bioengineering Division for publication in the JOURNAL OF BIOMECHANICAL ENGINEERING. Manuscript received by the Bioengineering Division May 19, 2003; revision received November 18, 2003. Associate Editor: A. Yoganathan.

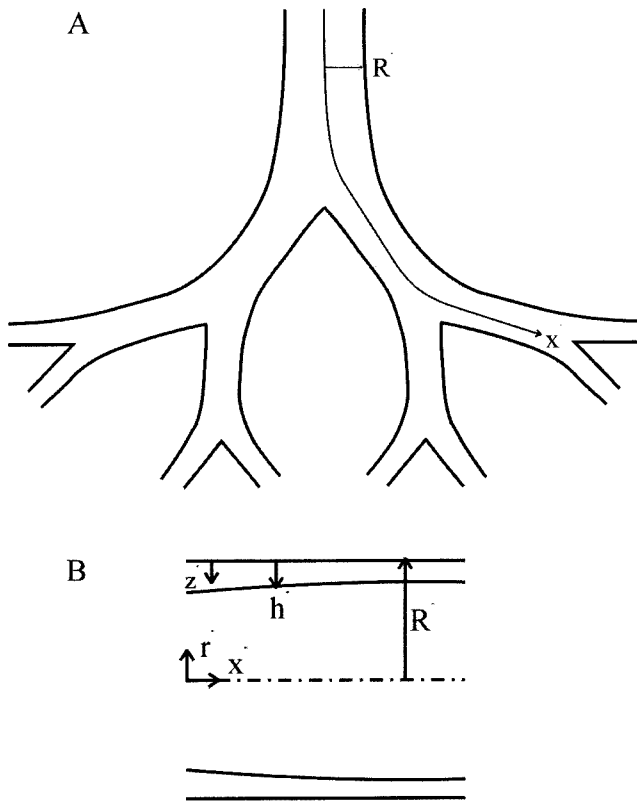


Fig. 1 (a) Branching network; (b) single tube. Here x^* is the axial position, R^* is the airway radius, r^* is the radial coordinate, z^* is the local radial coordinate relative to the wall, and h^* is the film thickness.

film is established prior to initiation of cycling. So in the uncycled state, there is a background transport of surfactant and liquid due to the Marangoni mechanism.

We study SRT by setting the proximal surfactant end condition to a value higher than the distal end. Then the system is perturbed with the wall cycling. Such movements affect the surfactant transport dynamics by several means including modification of the surfactant concentration gradients (and hence the surface tension gradients) and cycling of the film thickness (and hence viscous effects) for the entire film. A linear sorption interfacial kinetics equation is used to model the transport of surfactant from the bulk to the interface or vice versa. We derive and solve coupled non-linear evolution equations for film thickness, surfactant surface concentration, and surfactant bulk concentration. From these equations we can calculate the axial surfactant and liquid fluxes.

1 Model

1.1 Governing Equations. In our model, we make some simplifying assumptions based on the geometry of airways of the lung and the properties of the thin liquid layer coating the inner surface of the airways. The airway tree consists of a branching network of tubes, whose total perimeter increases with airway generation due to branching, as shown in Fig. 1(a). This axial perimeter growth can be modeled by introducing a total airway perimeter function into the governing equations. To model breathing, we allow each individual airway to expand and contract cyclically in the radial and axial directions. Since the film thickness is small compared to the airway radius and circumferential concentration gradients are neglected, there will not be any circumferential flows and the flow and concentration fields are not functions of the azimuthal coordinate.

Consider a thin viscous film lining a branching, stretchable, membrane tube as in Fig. 1(b), where $R^*(x^*, t^*)$ is the radius of an individual tube (airway), with x^* representing the path length along the airway and t^* denoting time. The z^* -axis extends outward from the membrane wall towards the center of the airway. Note that variables with stars are dimensional, and parameters and dimensionless variables are un-starred. The fluid domain is bounded by the distal end of the branching tree, $x^* = L^*(t^*)$, and the proximal end, $x^* = 0$. The position of the film surface is defined as $z^* = h^*(x^*, t^*)$, the surface concentration of the soluble (in general) surfactant is denoted by $\Gamma^*(x^*, t^*)$, and the bulk concentration of surfactant is denoted by $c^*(x^*, z^*, t^*)$.

1.2 Lung Morphometry. The area expansion due to branching is accounted for by allowing the total perimeter (of each individual tube summed over the entire number of tubes at a given location along the airway tree) of the branching membrane tube to vary with x^* (see Fig. 1(a)). The dimensional perimeter, given by $b^*(x^*, t^*)$, is determined from a continuous version of the lung morphometry model [33]. The total airway perimeter, b_n^* , individual airway radius, R_n^* , and individual airway length, l_n^* , at airway generation n are given by

$$b_n^* = b_0 2^{2n/3}, \quad R_n^* = R_0 2^{-n/3}, \quad l_n^* = l_0 2^{-n/3} \quad (1)$$

where b_0 , R_0 , and l_0 represent the tracheal (airway generation 0) perimeter, radius and length, respectively. Let the discrete variable x_n^* denote the distance from the tracheal carina to the end of generation n :

$$x_n^* = -l_0^* + \sum_{m=0}^n l_m^* = \hat{L}_0 (1 - 2^{-n/3}) \quad (2)$$

where total path length is $\hat{L}_0 = l_0 / (2^{1/3} - 1)$. Using Eq. (2), n is eliminated from Eq. (1) and the discrete variable x_n^* is replaced by the continuous variable x^* to obtain the following expressions for the perimeter and airway radius for the case of no stretch:

$$b^*(x^*) = \frac{b_0}{(1 - x^*/\hat{L}_0)^2}, \quad R^*(x^*) = R_0 (1 - x^*/\hat{L}_0). \quad (3)$$

Below, we introduce wall stretch into a similar expression for $b^*(x^*, t^*)$, where we measure x^* from generation 7 rather than the trachea [11]. Generation 7 is the start of the Marangoni domain, and the thick layer of surfactant in the larger airways feeds the surfactant monolayer that exists from generation 7 to the alveoli. We have not taken into account mucus rheology since the ratio of mucus to periciliary liquid is small in the distal airways of the lung [34]. The dimensional airway radius, $R^*(x^*, t^*)$, of each airway is determined in a similar manner. The branching membrane tube is periodically stretched in the x^* and r^* directions to mimic elongation and radial stretch of the airways during breathing.

1.3 Governing Equations for a Single Airway. We will initially consider an individual tube that is oscillated in length and radius (see Fig. 1(b)), and later in this section we will consider the full branching network of tubes. The governing equations for conservation of linear momentum (the Navier-Stokes equation), and the conservation of fluid mass are

$$\rho \left(\frac{\partial \mathbf{v}^*}{\partial t^*} + \mathbf{v}^* \cdot \nabla^* \mathbf{v}^* \right) = -\nabla^* p^* + \mu \nabla^{*2} \mathbf{v}^*, \quad \nabla^* \cdot \mathbf{v}^* = 0 \quad (4)$$

where \mathbf{v}^* is the velocity vector in the global reference frame, ∇^* is the gradient operator and p^* is pressure. For conservation of the surfactant species on the interface we have the surface transport equation

$$\frac{\partial \Gamma^*}{\partial t^*} + \nabla_s^* \cdot (\mathbf{v}_s^* \Gamma^*) - D_s \nabla_s^{*2} \Gamma^* + (\nabla_s^* \cdot \mathbf{n})(\mathbf{n} \cdot \mathbf{v}^*) \Gamma^* - J^* = 0 \quad (5)$$

where $\nabla_s^* \equiv (\mathbf{I} - \mathbf{nn}) \cdot \nabla^*$ is the surface gradient operator, \mathbf{n} is the surface normal, \mathbf{I} is the identity tensor (with components I_{ij} such that $I_{ij} = 1$ if $i = j$ and $I_{ij} = 0$ if $i \neq j$), $\mathbf{v}_s^* \equiv (\mathbf{I} - \mathbf{nn}) \cdot \mathbf{v}^*$ is the surface velocity, and J^* is the flux of surfactant from the bulk to the interface. The surfactant may diffuse along the interface with constant diffusivity, D_s , as well as be convected along the surface. For conservation of surfactant species in the bulk phase, we have the bulk transport equation

$$\frac{\partial c^*}{\partial t^*} + \nabla^* \cdot (\mathbf{v}^* c^*) = D_b \nabla^{*2} c^* \quad (6)$$

where D_b is the bulk diffusivity.

A linear equation of state that relates the surface tension to the surfactant concentration is used:

$$\sigma^* = \sigma_m + \left(\frac{\partial \sigma^*}{\partial \Gamma^*} \right) \Big|_{\Gamma^* = \Gamma_m} (\Gamma^* - \Gamma_m) \quad (7)$$

where Γ_m is the maximum initial surface concentration in the new surfactant region, and σ_m is the corresponding surface tension.

The interfacial and bulk concentrations of surfactant are coupled through J^* , the flux out of the fluid, which is given by

$$J^* = -[D_b(\mathbf{n} \cdot \nabla^*)c^*]_s \quad (8)$$

The flux of surfactant between the bulk and the interface is determined using linear sorption kinetics, where the adsorption of surfactant to the surface varies linearly with the bulk concentration, c^* , and the desorption from the surface varies linearly with the surface concentration, Γ^* . Thus, the flux can be written as

$$J^*(\Gamma^*, c_s^*) = k_1 c_s^* - k_2 \Gamma^* \quad (9)$$

where c_s^* is the bulk concentration just below the interface. A more complicated model of the surfactant flux between the bulk and interface is one that incorporates squeeze-out [35]. The premise of such a model is that the surface concentration cannot exceed a certain maximum value (which we will take to be Γ_m when using this method), even under compression. If the interface is compressed further after Γ_m has been achieved, Γ^* will not increase; rather surfactant will be squeezed from the interface into the bulk. We considered this sorption kinetics model, but the results obtained using it are not presented here in the interest of brevity since the results were not significantly different from the linear sorption results. There are other sorption kinetics models that have been shown to provide good agreement with experiments, e.g. Frumkin and double layer [36].

In this model, we allow the individual airways to stretch radially and longitudinally with a strain field specified by the airway perimeter, $b^*(x^*, t^*)$, and wall velocity, $V_{wall}^*(x^*, t^*)$, but consider the concentration field to be azimuthally symmetric and thus consider no flow in the azimuthal direction. The velocity vector, $\mathbf{v}^* = (u^*, 0, w^*)$, in a frame of reference fixed with the moving tube wall, satisfies the no slip and no penetration conditions, so that

$$u^*(x^*, z^* = 0, t^*) = V_{wall}^*(x^*, t^*), \quad w^*(x^*, z^* = 0, t^*) = 0. \quad (10)$$

At the air-liquid interface, $z^* = h^*(x^*, t^*)$, the jump in tangential and normal stresses boundary conditions due to the presence of surfactant and a kinematic boundary condition are applied:

$$[t_i T_{ij}^* n_j] = \frac{\partial \sigma^*}{\partial s^*}, \quad [n_i T_{ij}^* n_j] = \sigma^* \kappa^*, \quad \frac{\partial h^*}{\partial t^*} = -\frac{\partial Q^*}{\partial x^*} \quad (11)$$

where $T_{ij}^* = -p \delta_{ij} + \mu(\partial u_i^*/\partial x_j^* + \partial u_j^*/\partial x_i^*)$ is the stress tensor, δ_{ij} is the Kronecker delta tensor, \mathbf{n} and \mathbf{t} are the normal and tangent vectors, κ^* is the interfacial curvature, $\partial \sigma^*/\partial s^*$ is the directional-derivative of surface tension along the interface and $Q^*(x^*, t^*) = \int_0^{h^*} u^* dz^*$ is the axial flow rate per unit circumference.

Appropriate boundary values for film thickness, and surface and bulk surfactant concentrations at the distal boundary of the film, $x^* = L^*(t^*)$, and the proximal boundary of the film, $x^* = 0$, are discussed below.

In the film the axial coordinate is scaled with respect to L_0 , the cycle mean path length of the lung (from generation 7 to 18), so that $x = x^*/L_0$, and the local radial coordinate is scaled with respect to h_0 , the film thickness at $x^* = 0$, so that $z = z^*/h_0$. The velocity scale $U = M \sigma_m h_0 / (\mu L_0)$ is obtained by balancing the viscous stress and surface tension gradient that appear in the tangential stress condition (11), where $M = (-\partial \sigma^*/\partial \Gamma^*)|_{\Gamma^* = \Gamma_m} \Gamma_m / \sigma_m$ is an elasticity number that provides a measure of surfactant activity, so that Eq. (7) becomes $\sigma = 1 - M(\Gamma - 1)$. Then $u = u^*/U$ and $w = w^*/(\varepsilon U)$ where $\varepsilon = h_0/L_0$. Also, $t = t^*/T_V$, where $T_V = L_0/U$ is the viscous-surface tension time scale, and $p = p^*/(\sigma_m/h_0)$. The surfactant concentration is scaled with respect to Γ_m , the maximum initial surface concentration in the new surfactant region. The scaling of c^* is obtained by setting $J^* = 0$ in and is $\hat{c} = k_2 \Gamma_m / k_1$.

We employ lubrication analysis by taking the limit of $\varepsilon \rightarrow 0$ (as is the case physiologically and experimentally). In this limit, terms of $O(\varepsilon^2 \text{Re})$ and $O(\varepsilon^2)$ from the momentum equation, Eq. (4), and the interfacial stress boundary condition, Eq. (11), are negligible. Also, we assume that the change in radius over the length of an individual airway is small. [Note that this approximation is not to be confused with the dilution effect which is modeled using the perimeter function $b^*(x^*, t^*)$]. Thus, we obtain to leading order

$$\begin{aligned} u_{zz} &= \frac{1}{M} p_x, \\ p_z &= 0, \\ p|_{z=h} &= -(1 - M(\Gamma - 1)) \left(\frac{\phi}{R - \phi h} + \varepsilon^2 h_{xx} \right), \\ u_z|_{z=h} &= -\Gamma_x, \end{aligned} \quad (12)$$

from the x -component of the Navier-Stokes equation, the z -component of the Navier-Stokes equation, the normal stress boundary condition, and the tangential stress boundary condition, respectively. Here $\phi = h_0/r_0$ is the ratio of the film thickness to tube radius at generation 7. Integrating Eq. (12), twice gives

$$u = \frac{1}{2M} p_x (z^2 - 2hz) - \Gamma_x z + V_{wall} \quad (13)$$

where $V_{wall}(x, t) = V_{wall}^*/U$ is the non-dimensional wall velocity of the membrane.

1.4 Branching Network Equations. Up to this point our model formulation has considered a single airway. We now incorporate the effects of perimeter expansion (airway branching) into the model. The classical kinematic boundary condition is modified here to take into account the variation of perimeter with axial distance x . Consider a fluid volume element, V_{fluid} , bounded by x and $x + \Delta x$. Mass conservation requires that the time rate of change in fluid volume is equal to the difference between the inflow and outflow, such that

$$\frac{dV_{fluid}}{dt} \approx \frac{d}{dt} \int_x^{x+\Delta x} B(x, t) h(x, t) dx \approx [-B(x, t) Q(x, t)]_x^{x+\Delta x} \quad (14)$$

where $B(x,t)$ is the dimensionless perimeter ($b^*(x^*,t^*)$ divided by the perimeter at generation 7), and $Q(x,t)$ is the axial flowrate per unit circumference corresponding to a single airway at the axial location x . We have assumed here that the characteristic film thickness of the layer is much smaller than the tube radius. Thus, in the limit as $\Delta x \rightarrow 0$, the following evolution equation for the film thickness $h(x,t)$ is obtained

$$(Bh)_t + (BQ)_x = 0, \quad (15)$$

where, on using (13),

$$Q = -\frac{h^3}{3M}P_x - \frac{h^2}{2}\Gamma_x + hV_{wall}. \quad (16)$$

Similar arguments as above are applied to the conservation of surfactant species on the interface, yielding the following surface transport equation

$$(B\Gamma)_t + (Bq)_x - BJ = 0 \quad (17)$$

where q , the surface flux of surfactant is given by

$$q = -\frac{1}{Pe_s}\Gamma_x - \frac{1}{2M}P_x h^2 \Gamma - h\Gamma\Gamma_x + \Gamma V_{wall}. \quad (18)$$

In Eq. (18), $Pe_s = UL_0/D_s$ is the surface Péclet number, the ratio of transport due convection to that due to surface diffusion. In dimensionless form, the flux J , given by Eq. (9), is

$$J = \frac{1}{T_{D/V}}(c_s - \Gamma) \quad (19)$$

where $T_{D/V} = 1/(k_2 T_V)$ is the desorptive time scale. Recall, from Eq. (8) that the flux J can also be written in terms of the bulk concentration gradient at the interface:

$$J = -\frac{1}{\beta Pe_b} \left(\frac{1}{\varepsilon^2} c_z - h_x c_x \right) \Big|_{z=h} \quad (20)$$

where $\beta = \Gamma_{ref}/(h_0 \hat{c}) = k_1/(k_2 h_0)$ indicates the surface accumulation and substrate solubility of the surfactant [29,37], and $Pe_b = UL_0/D_b$ is the bulk Péclet number. An insoluble surfactant requires $\beta \rightarrow \infty$. In the limit $\beta \rightarrow 0$, the surfactant is highly soluble and there is weak surface accumulation. β is analogous to a Gibbs adsorption thickness, the ratio of the adsorptive length scale to the film thickness [37]. When $\beta \ll 1$, surfactant depletion in the bulk is minimal to reach equilibrium when the interface is expanded. When $\beta \gg 1$, a considerable amount of surfactant adsorbs to the interface to reach equilibrium upon surface expansion.

We consider rapid vertical diffusion through the liquid layer, $\varepsilon^2 Pe_b \ll 1$ and zero concentration gradient at the membrane wall [29] so that the bulk concentration can be represented by a term independent of z , the coordinate across the layer, plus a small fluctuation:

$$c(x,z,t) = c_0(x,t) + \varepsilon^2 P_b c_1(x,z,t) \quad (21)$$

where the cross-sectional average of c_1 is zero. We obtain the following leading order bulk surfactant transport equation using similar methods used to derive Eqs. (15) and (17):

$$(Bhc_0)_t = -(Bq_c)_x - B\beta J \quad (22)$$

where the leading order bulk surfactant transport q_c is given by

$$q_c = c_0 Q - \frac{1}{Pe_b} h c_{0x}. \quad (23)$$

1.5 Determination of Wall Velocity. For sinusoidal stretching of the wall, the position of the distal boundary varies with time as

$$L(t) = 1 + \Delta \sin\left(\frac{2\pi}{T_{C/V}}t\right) \quad (24)$$

where Δ is the amplitude of the periodic strain, and $T_{C/V} = T_C/T_V$ is the ratio of the period of oscillation of the membrane, T_C , to the viscous-surface tension time scale T_V . For uniform strain, the wall velocity field, V_{wall} , and the position of wall particles in the Eulerian reference frame are given by

$$V_{wall} = \xi \dot{L}(t), \quad x = \xi L(t). \quad (25)$$

Note ξ is a membrane wall material coordinate that is attached to the membrane wall and ranges from 0 to 1. We also allow the tube radius $R(x,t)$ and the tube perimeter function $B(x,t)$ to oscillate, by using

$$R(x,t) = \phi(1 - x_0 x/L(t)) \left(1 + \delta \sin\left(\frac{2\pi}{T_{C/V}}t\right) \right),$$

$$B(x,t) = \frac{1 + \delta \sin\left(\frac{2\pi}{T_{C/V}}t\right)}{(1 - x_0 x/L(t))^2} \quad (26)$$

where δ is the amplitude of the radial strain in the airway.

1.6 Initial and Boundary Conditions. After the initial transient spreading of the monolayer in the lung, the film height and surface concentration reach equilibrium values and there is a steady state flux of surfactant into the alveolar region, if breathing is neglected [11]. Using a similar approach as [11] to include the area expansion due to airway branching, we consider how breathing influences the flux of surfactant, which is soluble in this work, at later times. As the alveolar compartment kinetics regulate the surfactant concentration in the alveolus (approximately generation 18 in the lung morphometry model) and the instilled liquid forms a thicker region in the large airways that feeds the monolayer in the smaller airways, we use the following boundary conditions to model the transport at all but the initial transient spreading times.

Since the evolution equation for the film thickness is fourth order in x , four boundary conditions, two at $x=0$ and two at $x=L(t)$, need to be imposed:

$$h(0,t) = \frac{1}{1 + \delta \sin\left(\frac{2\pi}{T_{C/V}}t\right)}, \quad h_{xx}(0,t) = 0,$$

$$h(L(t),t) = \frac{h_1}{1 + \delta \sin\left(\frac{2\pi}{T_{C/V}}t\right)}, \quad h_{xx}(L(t),t) = 0. \quad (27)$$

The total cross-sectional area at either end of the domain is chosen to be fixed, so that $Bh = \text{constant}$ at $x=0$ and $x=L(t)$. The other two conditions, $h_{xx} = 0$, come from the requirement that the local fluid pressure is inversely proportional to the local radius of curvature. The boundary conditions for Γ and c_0 are as follows:

$$\Gamma(0,t) = \frac{1}{1 + \delta \sin\left(\frac{2\pi}{T_{C/V}}t\right)}, \quad c_0(0,t) = 1,$$

$$\Gamma(L(t),t) = \frac{\Gamma_1}{1 + \delta \sin\left(\frac{2\pi}{T_{C/V}}t\right)}, \quad c_0(L(t),t) = \Gamma_1. \quad (28)$$

The boundary conditions on Γ imply that the total interfacial surfactant mass is time independent at both ends of the domain. The bulk concentration is constant at either end of the domain so that the total surfactant mass $B(\Gamma + hc_0)$ is constant. The value of c_0 is determined by requiring that for no stretch $J=0$. In the absence of wall stretch, these boundary conditions allow steady transport of surfactant and liquid through the model domain and into the alveoli. Wall stretch results in a mean-steady transport of surfac-

tant and liquid through the domain. This is expected, as the instilled liquid in the larger airways supplies liquid and surfactant to the Marangoni region considered in this model.

We use the no-stretch, steady state values for h , Γ and c_0 as initial conditions for solving the evolution equations (15), (17) and (22). The no-stretch steady state profiles are obtained by solving the evolution equations numerically as described in the next section for $\delta=\Delta=0$. The code is then run until the total surfactant transport and the total liquid flux per cycle into the alveolar region asymptote to a steady value. This steady transport is then compared for different stretching parameters to assess which ventilation strategies might result in the most surfactant transport into the alveoli—the desired outcome of SRT. The time average surface surfactant transport, $\langle q_1 \rangle$, the bulk transport, $\langle S_1 \rangle$, and the fluid transport, $\langle Q_1 \rangle$, at $x=L$, are found by evaluating the following integrals

$$\begin{aligned} \langle q_1 \rangle &= \frac{1}{T_{C/V}} \int_t^{t+T_{C/V}} B q_{rel} dt \\ \langle S_1 \rangle &= \frac{1}{T_{C/V} \beta} \int_t^{t+T_{C/V}} B \left[c_0 Q_{rel} - \frac{h c_{0x}}{P e_b} \right] dt \\ \langle Q_1 \rangle &= \frac{1}{T_{C/V}} \int_t^{t+T_{C/V}} B Q_{rel} dt \end{aligned} \quad (29)$$

where the subscript “rel” indicates that the quantities are relative to the membrane wall, i.e. calculated from equations (16), (18) and (23) without the V_{wall} terms. These are computed for each cycle using $t=iT_{C/V}$ for $i=0,1,2,\dots$ until the value of the transport asymptotes to a constant mean steady value (taken to be when the value is within 10^{-6} of the previous value). Also, when the mean-steady state has been reached, $q(t)$ and $Q(t)$ at a given x coordinate repeat with a period $T_{C/V}$. We calculate the static transport values using

$$q_{1s} = \langle q_1(\Delta=0) \rangle, \quad S_{1s} = \langle S_1(\Delta=0) \rangle, \quad Q_{1s} = \langle Q_1(\Delta=0) \rangle. \quad (30)$$

We also estimate a characteristic velocity for SRT by computing the maximum cycle-averaged non-dimensional surface velocity relative to the membrane:

$$u_{char} = \left[\frac{1}{T_{C/V}} \int_t^{t+T_{C/V}} (u(x,h,t) - V_{wall}) dt \right]_{\max}. \quad (31)$$

1.7 Solution of the Evolution Equations. Next, we provide some estimates for the parameters that appear in the evolution equations and boundary conditions. A typical film thickness is $h_0=10^{-5}$ m [38,39], and the distance from generation 7 to generation 18 is approximately $L_0 \cdot 0.0274$ m [11]. The lung’s liquid lining is assumed to be a single Newtonian liquid layer. This is a reasonable approximation in the distal airways of the lung where the ratio of mucus to periciliary liquid is small [34]. Others have recently examined the effects of mucus rheology on surfactant spreading [40]. In addition, we have assumed that in these airways the liquid lining has approximately the same viscosity as water; thus $\mu=0.001$ kg m $^{-1}$ s $^{-1}$. We take the maximum surface tension to be that of a clean air-liquid interface, so that $\sigma_{\max}=0.07$ N m $^{-1}$. The critical bulk concentration is 0.8 kg m $^{-3}$ [41]. The maximum surface concentration for pulmonary surfactant is estimated to be 6×10^{-6} kg m $^{-2}$ [42]. We choose $\hat{c}=0.4$ kg m $^{-3}$ and $\Gamma_m=3 \times 10^{-6}$ kg m $^{-2}$. These values result in $\beta=0.75$ and $T_V \sim 1$ second. We set $P e_s=10^{10}$ and $P e_b=10^3$, consistent with small interfacial and bulk surfactant diffusivities. We use $T_{D/V}=60$, based on estimates that $T_D \sim 60$ seconds [35]. We choose $\Gamma_1=0.5$ and $h_1=0.2$ in the boundary conditions, Eqs. (27) and (28), so that for the case of no stretch and insoluble surfactant, we obtain almost the same steady state solutions that were found in [11]. In addition, we set $\phi=h_0/R_0=0.01$, ε

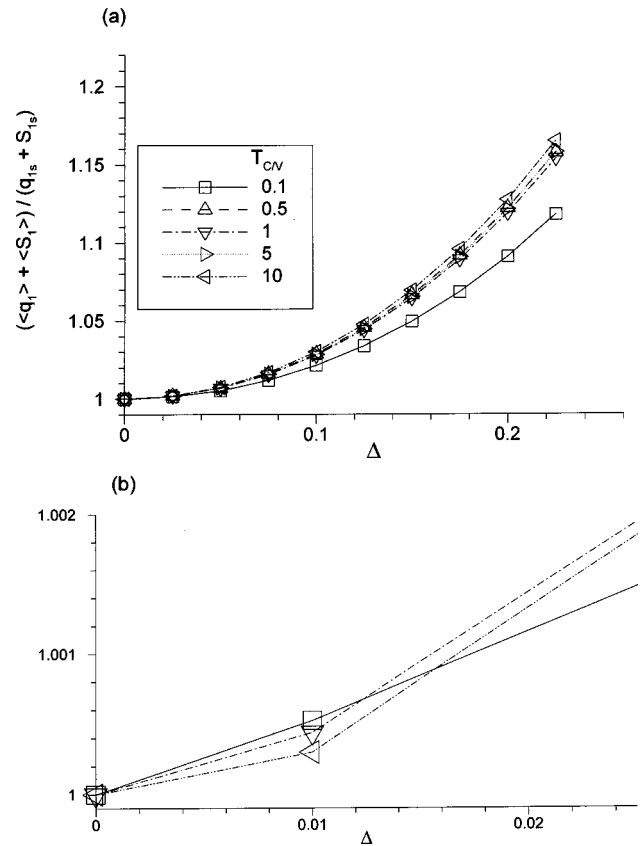


Fig. 2 Ratio of cycle averaged total surfactant flux at the distal end of the airways once a periodic state has been reached to its steady state value for the no stretch case.

$=h_0/L_0=0.001$ and the elasticity number $M=1$. We investigate various ventilation regimes, ranging from small to large tidal volumes, $0.05 \leq \Delta \leq 0.3$, and high to conventional frequency ventilation, $0.1 \leq T_{C/V} \leq 10$.

The systems to be solved consist of the coupled nonlinear evolution equations for h , Γ , and c_0 , Eqs. (15), (17) and (22), subject to: (i) the wall stretching kinematic boundary conditions of uniform strain, Eq. (25); (ii) the interfacial kinetics model of linear sorption, Eq. (19), and (iii) end conditions on film thickness and surfactant concentrations, Eqs. (27) and (28). The moving boundary of the domain can be treated by mapping x into a material coordinate, $\xi(x,t)$, such that constant ξ refers to a specific membrane particle, and using the chain rule of differentiation to transform the evolution equations in terms of the new coordinate. Thus, the grid points for the finite difference scheme used to solve the evolution equations are at fixed locations in ξ , but at varying locations in x , such that the boundary $x=L(t)$ corresponds to $\xi=1$ and is always at the last grid point. We transform the evolution equations to the new coordinate system, by

$$H(\xi, \tau) = h(x, t), \quad G(\xi, \tau) = \Gamma(x, t), \quad C(\xi, \tau) = c_0(x, t) \quad (32)$$

where ξ is given by Eq. (25). The system of evolution equations is solved using the method of lines, where the diffusive terms are approximated using central differences, the convective terms are approximated using a second order upwinding scheme [43], and the time-stepping part of the computation is performed using a backward difference method.

2 Results

Figure 2 shows total (surface plus bulk) surfactant transport (scaled by the steady-state no stretch values) into the alveoli ver-

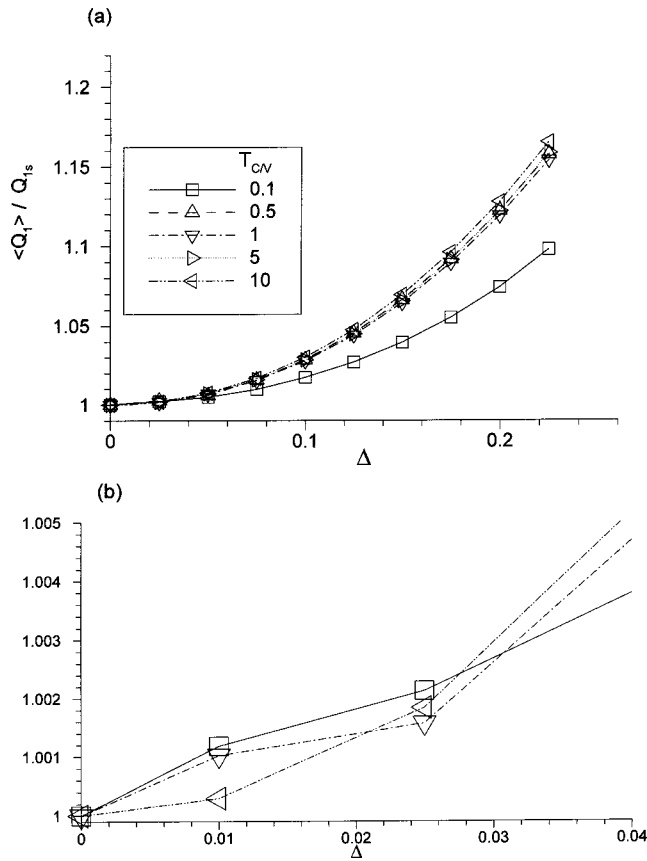


Fig. 3 Ratio of cycle averaged fluid flux at the distal end of the airways once a periodic state has been reached to its steady state value for the no stretch case.

strain amplitude, Δ . The total surfactant transport (surface and bulk), $(\langle S_1 \rangle + \langle q_1 \rangle) / (S_{1s} + Q_{1s})$ as in Eq. (29), into the alveoli increases quadratically with Δ , but is not strongly dependent on the breathing period T_{CV} . For a fixed and small (large) value of Δ , decreasing T_{CV} , that is, increasing the breathing frequency results in increased (decreased) surfactant transport. The bottom panel of Fig. 2 shows the non-monotonic behavior of the total surfactant transport with respect to T_{CV} at small Δ . In these calculations, the cycle averaged interfacial surfactant transport $\langle q_1 \rangle$ is larger than the cycle averaged bulk surfactant transport $\langle S_1 \rangle$ because the surface velocity is, on average, larger than the cross-sectionally averaged axial velocity.

The cycle averaged transport of liquid into the alveolar region, $\langle Q_1 \rangle / Q_{1s}$ evaluated using Eq. (29), also increases quadratically with Δ (Fig. 3). Varying T_{CV} has a smaller effect, but its impact on $\langle Q_1 \rangle$ is more significant than on $\langle S_1 \rangle + \langle q_1 \rangle$. As for surfactant transport, liquid transport increases with cycle frequency for small values of strain amplitudes.

Figure 4 shows both the surfactant and liquid transport versus time, at the proximal (a and c) and distal (b and d) ends for several period values, after the mean-steady regime has been reached, with $\Delta = 0.1$. Note that for given Δ and T_{CV} , the steady state cycle averaged transport values are the same at the proximal and distal ends, and for $\Delta = 0.1$ the transport is weakly dependent on T_{CV} (Figs. 2 and 3). Also shown in Fig. 4 is the membrane length, $L(t)$, to give an indication of the phase of the transport relative to the periodic wall stretch. Transport at the proximal end is approximately $\pi/2$ out of phase with the membrane stretch while transport at the distal end is out of phase by $-\pi/2$. Also, the amplitude of the fluxes increases with frequency. At large frequencies, for example $T_{CV} = 0.1$, the flux amplitudes at the distal end can be an order of magnitude larger than those at the proximal end.

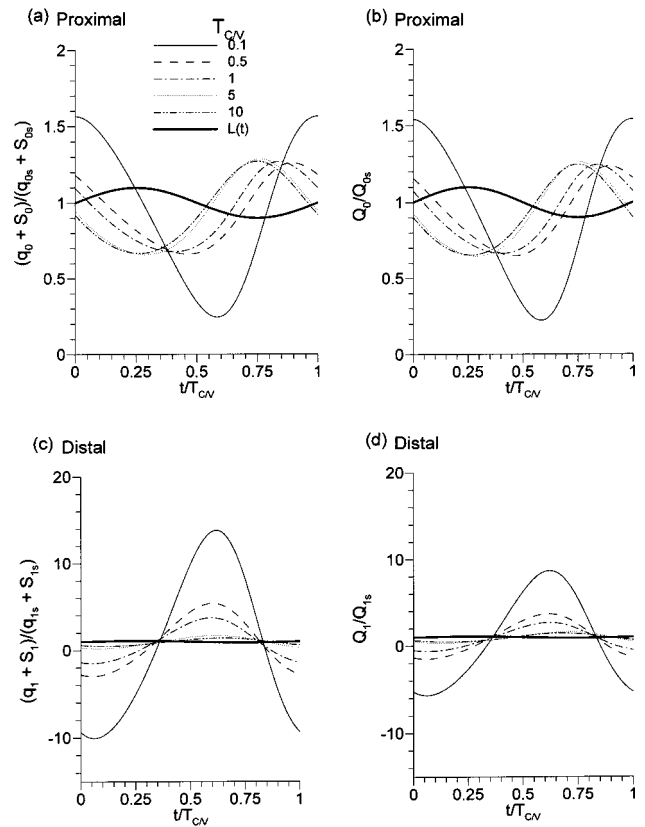


Fig. 4 Transport versus time once a periodic steady state has been reached. Proximal end: (a) total surfactant transport, (b) liquid transport. Distal end: (c) total surfactant transport, (d) liquid transport. Here $\Delta = 0.1$.

In Fig. 5(a)–(h) the flow field within the liquid layer is shown in a frame of reference fixed with the moving wall at various times during one period of oscillation once the time periodic steady state has been reached for the case where $\Delta = 0.1$ and $T_{CV} = 1$. This corresponds to a case where the viscous time scale is equal to the period of the wall stretch. A series of waves are observed to develop in the film, which propagate toward the distal end of the membrane. During the first quarter of the cycle, the membrane elongates from its mean value of $\langle L(t) \rangle = 1$, corresponding to mid-inspiration, and the film thins, consistent with the boundary conditions (see Eq. (27)). The flow close to the interface has a small streamwise component towards the distal end near $x = 0$ indicating the relative strength of the Marangoni-induced flow near the proximal end which diminishes (with respect to the membrane velocity) as x increases towards $x = L(t)$. The vertical component of velocity in the layer is mostly negative consistent with the thinning of the film during this initial part of the period. Also, note that near the membrane wall, there is a small velocity component towards the proximal end. At $t = T_{CV}/4$, when the membrane velocity is zero, the flow is mostly from left to right, and dominated at the proximal end by the Marangoni effect (Fig. 5(c)). The membrane contracts (and the film thickens) during $T_{CV}/4 \leq t \leq 3T_{CV}/4$ reaching a maximum velocity toward the proximal end at $t = T_{CV}/2$. In Figs. 5(d)–(f) the vertical component of velocity is mostly positive, and for sufficiently large x the flow near the interface is toward the interfacial waves. In addition, the streamwise velocity component in the moving frame is mostly positive. The membrane wall motion compresses the interface resulting in an increase in the interfacial surfactant concentration (see Fig. 8(a) below). This is more pronounced at the proximal end of the domain, causing this positive velocity component. The steady streamlines displayed in Fig. 5(i) show that the flow is on

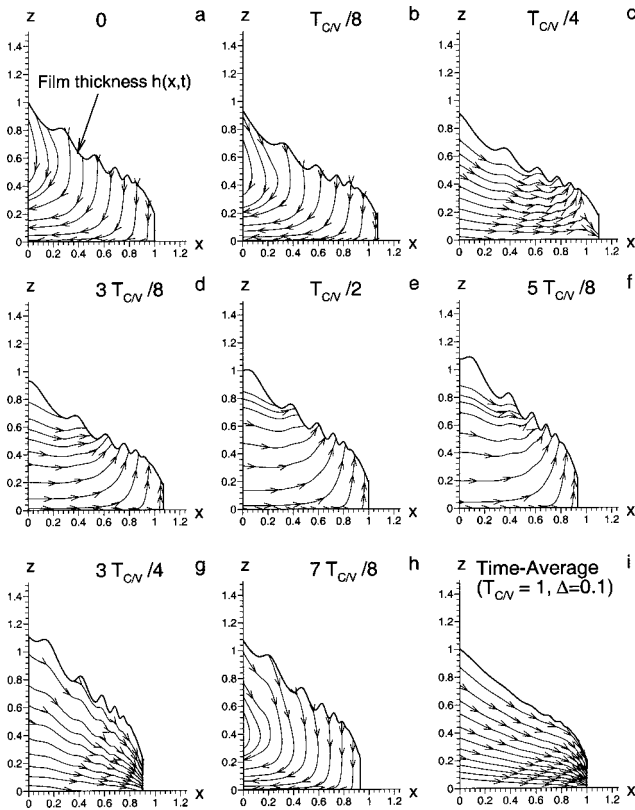


Fig. 5 Velocity field within film layer over one cycle once the steady periodic state has been reached, a $t = t_0 + t_i$ where $t_i = (a) 0; (b) T_{CV}/8; (c) T_{CV}/4; (d) 3T_{CV}/8; (e) T_{CV}/2; (f) 5T_{CV}/8; (g) 3T_{CV}/4; (h) 7T_{CV}/8$. The cycle averaged field is shown in (i). Here the amplitude is $\Delta = 0.1$, the stretch cycle is $T_{CV} = 1$ and t_0 is a sufficiently large enough value so that the steady-state has been reached.

the average towards the distal end of the membrane. Note that when the membrane is not stretched there is also a net flow towards the distal end of the membrane.

In Fig. 6, the flow field in the liquid layer is shown for a cycling period $T_{CV} = 10$ and an amplitude $\Delta = 0.1$. This corresponds to a tenfold increase in T_{CV} compared with the case shown in Fig. 5. In the limit $T_C \gg T_V$, the viscous-surface tension is much shorter than the time scale for wall motion, and the system behaves like the steady case [11]. At any instant in time, the film responds to the imposed surfactant gradient across the domain, given some fixed wall velocity. The surface waves have completely disappeared, and the film thickness is now a monotonic function of distance x . At all times during the cycle, the horizontal velocity is positive almost everywhere in the layer demonstrating that for this particular choice of parameters the Marangoni effect is dominant. During the expansion phase, there is still a region of weak retrograde flow near the membrane wall, but its size diminishes with decreasing T_{CV} (compare, for example, Figs. 5(a) and 6(a)).

At high frequencies, when the flow in the layer is dominated by the motion of the membrane (see Fig. 7 with $T_{CV} = 0.1$ and $\Delta = 0.1$), a small train of waves are observed to propagate from the proximal to the distal end, but attenuate relatively quickly, unlike the case $T_{CV} = 1$ (Fig. 5). During the expansion phase (panels a-b and panel h) the axial velocity in the frame of reference fixed to the membrane is towards the proximal end, while during the contraction phase (panels d, e and f) the axial velocity is towards the distal end. However, when the membrane stops stretching or contracting as in Figs. 7(c) and (g) the flow is mostly towards the distal end because of the negative surfactant gradient across the domain.

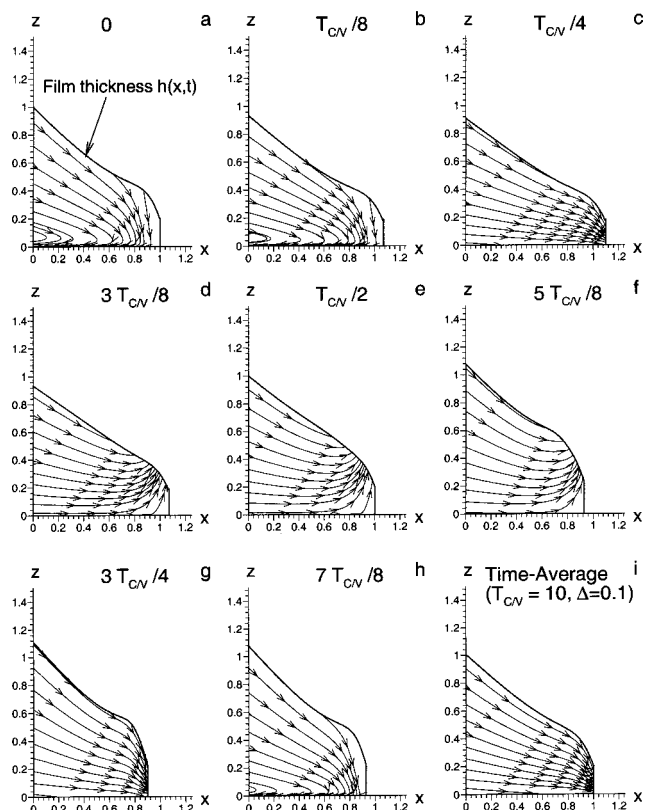


Fig. 6 The influence of increasing the stretch cycle to $T_{CV} = 10$ on the flow field within the liquid layer during a cycle. The values of t_i are the same as those given in the caption of Figure 5.

In Fig. 8, we plot the variation of the interfacial surfactant concentration Γ with distance x corresponding to the flow fields and film heights shown in Figs. 5–7 for $T_{CV} = 1, 10, 0.1$. Γ decreases with x over most of the domain. At low cycling frequencies (Figs. 8(a) and (b)), the surfactant gradient becomes quite shallow at the distal end due to dilution effects. Fig. 8(a) indicates that during the expansion phase Γ develops a local minimum at the distal end and so there must be a weak surfactant gradient driving flow towards the proximal end. The existence of the local minimum is similar to that observed for steady flows [11]. At the distal end, the surfactant gradient can be rather small because of the tremendous increase in surface-area. However, other effects such as the pressure-driven flow due to changes in airway diameter, which can result in the convection of endogenous surfactant towards the distal end, and the membrane motion that results in surface area changes, become more important at the distal end, and can in turn produce this local minimum in surfactant concentration. For short periods ($T_{CV} < 1$), as shown in Fig. 8(c), there is a substantial increase in the gradient of Γ at the distal end of the domain because of the increased compression of the interface. When the membrane is shortening $\partial\Gamma/\partial x|_{x=L} < 0$, and when it is lengthening $\partial\Gamma/\partial x|_{x=L} > 0$. For longer periods, Γ depends on the membrane length, but not on whether the membrane is lengthening or shortening.

We have not shown here profiles for the bulk concentration since the surfactant is relatively insoluble. The bulk surfactant concentration is essentially equal to its boundary value at $x = 0$ over most of the domain, and then decreases over a relatively short distance to its boundary value at $x = L(t)$ because $Pe_b \gg 1$.

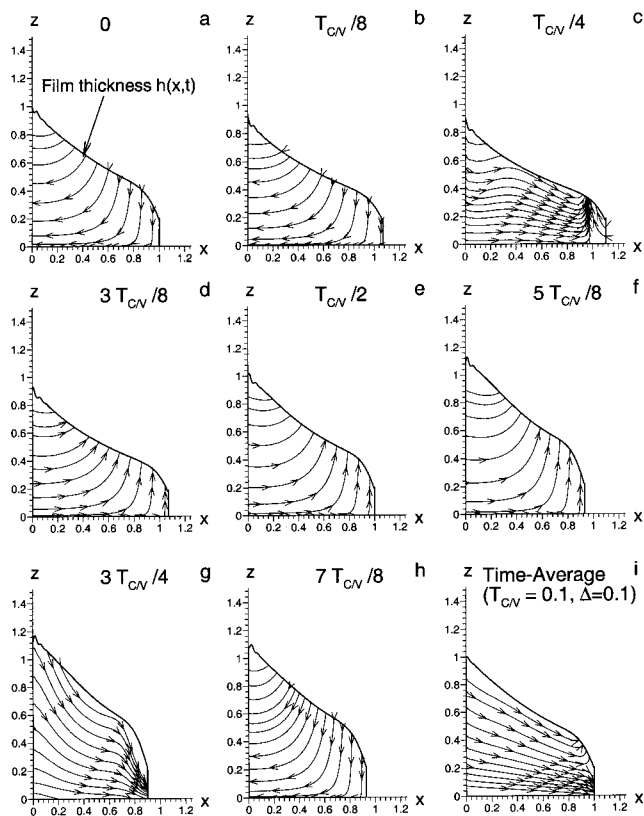


Fig. 7 The influence of high frequency membrane cycling on the flow field within the liquid layer during a cycle. Here $T_{CV} = 0.1$. The values of t , are the same as those given in the caption of Figure 5.

3 Discussion

The surfactant transport is considerably more dependent on strain amplitude, Δ , than on oscillation period (see Figs. 2 and 3). Typically, the “minute ventilation” (the total volume of air leaving the lung each minute~the product of frequency and tidal volume) is held constant when changing ventilation schemes for patients on ventilators [44], such as in SRT patients. For a fixed minute ventilation, a slower breathing frequency (longer period) allows a larger tidal volume (strain amplitude) per breath. This suggests that larger tidal volumes and larger breathing cycle periods would result in greater surfactant transport into the alveolar region than small tidal volumes and small breathing periods. Clinically, this is important, as the goal of SRT is to reduce the alveolar surface tension by transporting a large amount of exogenous surfactant into the alveoli quickly. There may be other considerations regarding the mode of ventilation, such as ventilator induced lung injury [45–47]. The compression and expansion of the interface coupled to the concomitant compression and expansion of the surfactant molecules on the interface induce interfacial waves. The effects of these waves could be significant with regards to airway closure, as thicker films result in less time to airway closure [48].

To better understand SRT transport’s weak dependence on cycling period and much stronger dependence on strain amplitude, it should be first noted that the cycle averaged boundary conditions for h and Γ , Eqs. (27) and (28), are inversely proportionally to $(1 - \Delta^2)^{1/2}$, which implies that increasing the strain amplitude Δ causes a rise in the time average film thickness and surfactant concentration at the boundaries. The film thickness changes influence the transport of surfactant and liquid by changing the viscous resistance, with a thicker film offering less resistance. In Fig. 7 the film is cycled more quickly ($T_{CV} = 0.1$) than the case shown in

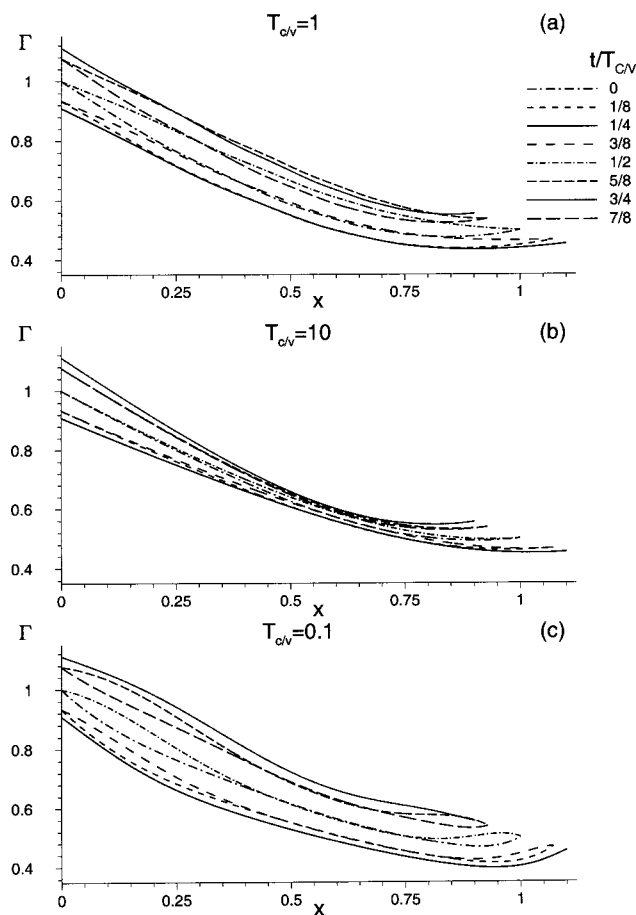


Fig. 8 Influence of stretching cycle on the surface surfactant concentration, Γ , plotted here versus axial position, x , at different times in stretching cycle. (a) $T_{CV} = 1$, (b) $T_{CV} = 10$, (c) $T_{CV} = 0.1$. Here $\Delta = 0.1$.

Fig. 6 ($T_{CV} = 10$). The onset of flow reversal (towards the proximal end) begins much earlier at higher frequencies, even before membrane begins to contract (see for example, Fig. 7(c)). Also, during the contraction phase, the flow within the film layer can be directed towards $x = 0$ only. At the higher frequency (Fig 7(i)), the cycle averaged flow contains a small region of flow away from the proximal end at $x = 1$, and this may contribute to the slight reduction in liquid and surfactant transport compared with the lower frequency case (Fig. 6(i)). At low frequencies, the surfactant gradient is rather small at the distal end because of the tremendous increase in surface-area. However, other effects such as the pressure-driven flow due to changes in airway diameter and the membrane motion become more important at the distal end, and can in turn produce a local minimum in surfactant concentration. The surface concentration of surfactant has larger fluctuations near the distal end of the membrane when the cycling period is short (Fig. 8(c)). The gradients in surface concentration at the distal end of the membrane can be quite large for small T_{CV} . As the boundary conditions specify the value of Γ at both ends of the domain, the spatial gradient of Γ changes greatly with time when the membrane is cycled quickly. At some times during the cycle, the gradient at the distal end opposes the large-scale flow into the alveolar region, contributing to the lack of frequency dependence at high frequencies. When the cycle period is longer, the gradient does not change as much with time. Cycling the membrane at a slower frequency provides more time for surfactant to adsorb to the interface. Consequently, the fluctuations of Γ at the distal end are not as large for long cycling periods. Despite these differences

in surface concentration gradients for different values of $T_{C/V}$, the cycle-averaged transport does not vary much with $T_{C/V}$ as the viscous resistance at the distal end also depends on $T_{C/V}$.

We can estimate a characteristic dimensional velocity for surfactant replacement therapy by computing the cycle-averaged surface velocity u_{char} given by Eq. (31). This value is converted to a dimensional one using $\sigma_{max} \approx 0.07 \text{ N m}^{-1}$, $h_0 \approx 10^{-5} \text{ m}$, $L_0 \approx 0.0274 \text{ m}$ (the distance from generation 7 to generation 18) and $\mu = 0.001 \text{ kg m}^{-1} \text{ s}^{-1}$ (the viscosity of water). This results in a characteristic velocity of 0.025 m s^{-1} at the proximal end ($x=0$), using an amplitude $\Delta=0.1$ and a cycle period $T_{C/V}=1$ in the computational model. At the distal end ($x=L(t)$), the characteristic velocity is two orders of magnitude smaller than the value at the proximal end. From Eq. (25), the maximum dimensional wall velocity is $V_{men} = 2 \pi \Delta L_0 / (T_{C/V} T_V)$ where $T_V = L_0 / U$. For $\Delta=0.1$ and $T_{C/V}=1$ $V_{men} = 0.016 \text{ m s}^{-1}$. Thus, the Marangoni-induced flow can be sufficiently large to overcome the wall motion especially at the proximal end. Espinosa & Kamm [32] found that for nonlinear strain and a wall with no perimeter variations, wall motion causes fluid motion in the opposite direction.

The bulk concentration profile changes significantly at the distal end because of the choice of the boundary condition values used at the proximal and distal ends, and the smallness of the bulk Péclet number. We found (but not shown in this paper) that varying Pe_b in the range $10^2 \leq Pe_b \leq 10^5$ had little effect on both surfactant and liquid transport. When $T_C \ll T_D$, there is simply not enough time for the surfactant on the surface to enter the bulk or the surfactant in the bulk to reach the surface due to the sorption kinetics. However, when T_C is larger, compressing the membrane results in surfactant leaving the surface and entering the bulk fluid. The bulk concentration gradient is steeper at the distal end for larger $T_{C/V}$. Unlike very small values of $T_{C/V}$, the longer cycling periods allow sufficient time for surfactant to adsorb to the air-liquid interface. However, these features do not cause the cycle-averaged transport of surfactant and liquid to be greatly period dependent. There is strain amplitude dependence since the strain amplitude influences the magnitude of film thickness and surfactant concentration changes.

3.1 Limitations of the Model. We have presented a model of SRT that retains the physiologically relevant features. However, future models could include such effects as air friction on the liquid layer, and variations in the relative inspiration/expiration portions of the breathing cycle. While we do not expect the previously mentioned items to have large effects on the results, a better understanding of the strain field in the airways, a more realistic sorption kinetics model, and accounting for surfactant degradation would improve the physiological accuracy of future models. We have neglected fluid sources and sinks within the domain. In fact, liquid enters the airways through the wall in a manner that most likely depends on local wall strain. This would likely change the film thickness. Gravity drainage is neglected. These effects would be important if the film thickness increased substantially such that airway closure could occur. For large strain amplitudes, a sorption kinetics model that more accurately describes lung surfactant [35,36] may be beneficial.

We have treated the respiratory tree as a continuous distribution in terms of total perimeter and radius of an individual airway, but we have ignored the potentially important effects at bifurcations. As a monolayer of surfactant spreads down the bronchial tree, differences in spreading rates could occur near an airway bifurcation. The liquid lining thickness may be non-uniform because of variations in airway wall curvature (see [49,50]). Entrance effects near the bifurcation could also play an important role in how surfactant distributes itself from a parent tube to the daughter branches [51].

Including the motion of cilia would also improve the models, as some cilia exist throughout the majority of the lung region considered here (typically to generation 16) [52]. Although the

smaller airways are less densely ciliated than the larger airways [53], cilia likely contribute to the flow in small airways as well. In our estimates of dimensional fluid velocities, we have used the viscosity of water and in our modeling have considered a homogeneous Newtonian fluid. In actuality, the viscosity may be higher than water and the fluid may be a mixture of Newtonian and non-Newtonian fluids due to the presence of mucus in or on top of the liquid lining of smaller airways. Mucus is a non-Newtonian, viscoelastic gel whose apparent viscosity typically ranges from about 100 to 200,000 times the viscosity of water, depending on the rate of strain (higher rate of strain corresponds to lower apparent viscosity) [54]. The mucus layer is thought to be discontinuous or much thinner than the aqueous layer in small airways [34], and consequently it seems reasonable to omit its influence while first investigating the effects of wall stretch. A fluid bilayer could be used to model the aqueous layer and mucus layer [40]. The neglected convective and transient inertial terms (due to the oscillations) could be significant if the membrane is oscillated fast enough, which could occur in high frequency ventilation. Despite these possibilities for future improvements in the modeling of respiration effects on surfactant and liquid transport, our model provides good insight to how breathing influences surfactant and liquid transport.

3.2 Conclusions. The results presented here suggest that breathing could have a considerable impact on Marangoni-driven surfactant and liquid transport. While the transport of surfactant in SRT varies greatly with strain amplitude, Δ , the transport does not vary as much with the period of the oscillatory wall stretch, $T_{C/V}$, at a given Δ in our model of SRT. However, for a fixed minute ventilation, larger tidal volumes are possible when the breathing cycle period is longer. As the transport of surfactant into the alveolar region is considerably higher when Δ is large (≥ 0.2), it may be advantageous to use large tidal volumes and large breathing cycle periods with SRT to increase surfactant transport. The characteristic fluid velocity for SRT is $\sim 0.03 \text{ m s}^{-1}$ based on the viscosity of water. This is two orders of magnitude larger than estimates of the velocity imparted to the mucus by the cilia ($u_{cilia} \sim 0.0002 \text{ m s}^{-1}$ in the trachea) [55], partly due to our choice for the viscosity of the liquid layer, but it still suggests surfactant transport can be significant.

Our model can be modified to consider the clearance of surfactant and liquid from the lung by appropriately changing the surfactant boundary conditions at the proximal and distal ends of the lungs. This is currently being investigated.

Acknowledgments

This work was supported by NIH grant HL-41126 and NSF grants CTS-9412523 and DMS-0079478. We would also like to acknowledge the help of Dr. Hideki Fujioka.

References

- [1] Corbet, A., Bucciarelli, R., Goldman, S., Mammel, M., Wold, D., and Long, W., 1991, "Decreased mortality rate among small premature infants treated at birth with a single dose of synthetic surfactant: a multicenter controlled trial," *J. Pediatr. (St. Louis)*, **118**(2), pp. 277–284.
- [2] Kendig, J. W., Notter, R. H., Cox, C. et al., 1991, "A comparison of surfactant as immediate prophylaxis and as rescue therapy in newborns of less than 30 weeks gestation," *N. Engl. J. Med.*, **324**, pp. 865–871.
- [3] Long, W., Corbet, A., Cotton, R., Courtney, S., McGuinness, G., Walter, D., Watts, J., Smyth, J., Bard, H., and Chernick, V., 1991, "A controlled trial of synthetic surfactant in infants weighing 1250 g or more with respiratory distress syndrome. The American Exosurf Neonatal Study Group I, and the Canadian Exosurf Neonatal Study Group," *N. Engl. J. Med.*, **325**(24), pp. 1696–703.
- [4] Jobe, A. H., 1993, "Pulmonary surfactant therapy," *N. Engl. J. Med.*, **328**(12), pp. 861–868.
- [5] Fuhrman, B. P., Paczan, P. R., and DeFrancis, M., 1991, "Perfluorocarbon-associated gas exchange," *Crit. Care Med.*, **19**(5), pp. 712–22.
- [6] Wolfson, M. R., Greenspan, J. S., Deoras, K. S., Rubenstein, S. D., and Shaffer, T. H., 1992, "Comparison of gas and liquid ventilation: clinical, physiological, and histological correlates," *J. Appl. Physiol.*, **72**(3), pp. 1024–31.
- [7] Leach, C. L., Fuhrman, B. P., Morin, F. C., and Rath, M. G., 1993,

- "Perfluorocarbon-associated gas exchange (partial liquid ventilation) in respiratory distress syndrome: a prospective, randomized, controlled study," *Crit. Care Med.*, **21**(9), pp. 1270–8.
- [8] Tutuncu, A. S., Akpir, K., Mulder, P., Erdmann, W., and Lachmann, B., 1993, "Intratracheal perfluorocarbon administration as an aid in the ventilatory management of respiratory distress syndrome," *Anesthesiology*, **79**(5), pp. 1083–93.
- [9] Hirschl, R. B., Parent, A., Tooley, R., McCracken, M., Johnson, K., Shaffer, T. H., Wolfson, M. R., and Bartlett, R. H., 1995, "Liquid ventilation improves pulmonary function, gas exchange, and lung injury in a model of respiratory failure," *Ann. Surg.*, **221**(1), pp. 79–88.
- [10] Espinosa, F. F., and Kamm, R. D., 1998, "Meniscus formation during tracheal instillation of surfactant," *J. Appl. Physiol.*, **85**(1), pp. 266–72.
- [11] Halpern, D., Jensen, O. E., and Grotberg, J. B., 1998, "A theoretical study of surfactant and liquid delivery into the lung," *J. Appl. Physiol.*, **85**(1), pp. 333–352.
- [12] Espinosa, F. F., and Kamm, R. D., 1999, "Bolus dispersal through the lungs in surfactant replacement therapy," *J. Appl. Physiol.*, **86**(1), pp. 391–410.
- [13] Grotberg, J. B., Halpern, D., and Jensen, O. E., 1995, "Interaction of exogenous and endogenous surfactant: spreading-rate effects," *J. Appl. Physiol.*, **78**, pp. 750–756.
- [14] Gaver, D. P., and Grotberg, J. B., 1990, "The dynamics of a localized surfactant on a thin film," *J. Fluid Mech.*, **213**, pp. 127–148.
- [15] Troian, S. M., Herzolzheimer, E., and Safran, S. A. P. R. L., 1990, "Model for the fingering instability of spreading surfactant drops," *Phys. Rev. Lett.*, **65**, pp. 333–336.
- [16] Jensen, O. E., and Grotberg, J. B., 1992, "Insoluble surfactant spreading on a thin viscous film: shock evolution and film rupture," *J. Fluid Mech.*, **240**, pp. 259–288.
- [17] Espinosa, F. F., Shapiro, A. H., Fredberg, J. J., and Kamm, R. D., 1993, "Spreading of exogenous surfactant in an airway," *J. Appl. Physiol.*, **75**, pp. 2028–2039.
- [18] Siegfried, W., 1993, "Perspectives in gene therapy with recombinant adenoviruses," *Exp. Clin. Endocrinol.*, **101**(1), pp. 7–11.
- [19] Grotberg, J. B., 1994, Pulmonary flow and transport phenomena, In: *Ann. Rev. Fluid Mech.*, J. L. Lumley, M. Van Dyke, and H. L. Reed, eds, Annual Reviews, Inc., Palo Alto, pp. 529–571.
- [20] Jensen, O. E., Halpern, D., and Grotberg, J. B., 1994, "Transport of a passive solute by surfactant-driven flows," *Chem. Eng. Sci.*, **49**(8), pp. 1107–1117.
- [21] Bull, J. L., D. Halpern, and J. B. Grotberg, 1999, *The effect of time-periodic airway stretch on surfactant and liquid transport in the lung*, in *Interfaces for the Twenty-First Century*, Monterey, CA.
- [22] Bull, J. L., Nelson, L. K., Walsh, J. T., Glucksberg, M. R., Schurch, S., and Grotberg, J. B., 1999, "Surfactant-spreading and surface-compression disturbance on a thin viscous film," *J. Biomech. Eng.*, **121**(1), pp. 89–98.
- [23] Bull, J. L., and Grotberg, J. B., 2003, "Surfactant spreading on thin viscous films: film thickness evolution and periodic wall stretch," *Exp. Fluids*, **34**(1), pp. 1–15.
- [24] Jensen, O. E., 1998, "The stress singularity in surfactant-driven thin-film flows. Part 2. Inertial effects," *J. Fluid Mech.*, **372**, pp. 301–322.
- [25] Weh, L., and Linde, H., 1973, "Kraterrförmige Oberflächenströmungen in Anstrichfilmen, verursacht durch Silikonölzusätze," *Plaste Kautsch.*, **20**, pp. 849–860.
- [26] Keshgi, H. S., and Scriven, L. E., 1991, "Dewetting, nucleation and growth of dry regions," *Chem. Eng. Sci.*, **46**, pp. 519–26.
- [27] Gaver, D. P., and Grotberg, J. B., 1992, "Droplet spreading on a thin viscous film," *J. Fluid Mech.*, **235**, pp. 399–414.
- [28] Halpern, D., and Grotberg, J. B., 1992, "Dynamics and transport of a localized soluble surfactant on a thin film," *J. Fluid Mech.*, **237**, pp. 1–11.
- [29] Jensen, O. E., and Grotberg, J. B., 1993, "The spreading of heat or soluble surfactant along a thin liquid film," *Phys. Fluids A*, **5**(1), pp. 58–68.
- [30] Yih, C.-S., 1969, "Three-dimensional motion of a liquid film induced by surface-tension variation or gravity," *Phys. Fluids*, **12**(10), pp. 1982–1987.
- [31] Davis, S. H., Liu, A.-K., and Sealy, G. R., 1974, "Motion driven by surface-tension gradients in a tube lining," *J. Fluid Mech.*, **62**, pp. 737–751.
- [32] Espinosa, F. F., and Kamm, R. D., 1997, "Thin layer flows due to surface tension gradients over a membrane undergoing non-uniform, periodic strain," *Ann. Biomed. Eng.*, **25**(6), pp. 913–925.
- [33] Weibel, E. R. and D. M. Gomez, 1962, "Architecture of the human lung," *Science Wash. D.C.* **137**, pp. 577–585.
- [34] Sleight, M. A., 1991, Mucus Propulsion, In: *The Lung: Scientific Foundations*, R. G. Crystal and J. B. West, eds, Raven, New York, pp. 189–196.
- [35] Otis, Jr., D. R., Ingenito, E. P., Kamm, R. D., and Johnson, M., 1994, "Dynamic surface tension of surfactant TA: experiments and theory," *J. Appl. Physiol.*, **77**(6), pp. 2681–8.
- [36] Krueger, M. A., and Gaver, D. P., 2000, "A theoretical model of pulmonary surfactant multilayer collapse under oscillating area conditions," *J. Colloid Interface Sci.*, **229**, pp. 353–364.
- [37] Horn, L. W., and Davis, S. H., 1975, "Apparent surface tension hysteresis of a dynamical system," *J. Colloid Interface Sci.*, **51**, pp. 459–475.
- [38] Bastacky, J., Lee, C. Y., Goerke, J., Koushafar, H., Yager, D., Kenaga, L., Speed, T. P., Chen, Y., and Clements, J. A., 1995, "Alveolar lining layer is thin and continuous: low-temperature scanning electron microscopy of rat lung," *J. Appl. Physiol.*, **79**(5), pp. 1615–28.
- [39] Widdicombe, J., 1997, "Airway and alveolar permeability and surface liquid thickness: Theory," *J. Appl. Physiol.*, **82**(1), pp. 3–12.
- [40] Craster, R. V., and Matar, O. K., 2000, "Surfactant transport on mucus films," *J. Fluid Mech.*, **425**, pp. 235–258.
- [41] Ingenito, E. P., Mark, L., Morris, J., Espinosa, F. F., Kamm, R. D., and Johnson, M., 1999, "Biophysical characterization and modeling of lung surfactant components," *J. Appl. Physiol.*, **86**(5), pp. 1702–1714.
- [42] Schurch, S., Bachofen, H., Goerke, J., and Possmayer, F., 1989, "A captive bubble method reproduces the in situ behavior of lung surfactant monolayers," *J. Appl. Physiol.*, **67**, pp. 2389–2396.
- [43] Ferziger, J. H. and M. Peric, 2002, *Computational methods for fluid dynamics*, Berlin, Springer.
- [44] Slutsky, A. S., 1991, Mechanical Ventilation, In: *The Lung: Scientific Foundations*, R. G. Crystal and J. B. West, eds, Raven, New York, pp. 2163–2174.
- [45] Dreyfuss, D., and Saumon, G., 1998, "Ventilator-induced lung injury—Lessons from experimental studies," *Crit. Care Med.*, **157**(1), pp. 294–323.
- [46] Tremblay, L. N., and Slutsky, A. S., 1998, "Ventilator-induced injury: From barotrauma to biotrauma," *Proc. Assoc. Am. Physicians*, **110**(6), pp. 482–488.
- [47] Tremblay, L. N., A. S. Slutsky, D. Dreyfuss, and G. Saumon, 1998, Ventilator-induced lung injury: mechanisms and clinical correlates, In: *Physiological basis of ventilatory support*, J. J. Marini and A. S. Slutsky, eds, Marcel Dekker, New York, pp. 395–451.
- [48] Halpern, D., and Grotberg, J. B., 1993, "Surfactant effects on fluid-elastic instabilities of liquid-lined flexible tubes: a model of airway closure," *J. Biomech. Eng.*, **115**(3), pp. 271–277.
- [49] Jensen, O. E., 1997, "The thin liquid lining of a weakly curved cylindrical tube," *J. Fluid Mech.*, **331**, pp. 373–403.
- [50] Rosenzweig, J., and Jensen, O. E., 2002, "Capillary-elastic instabilities of liquid-lined lung airways," *J. Biomech. Eng.*, **124**(6), pp. 650–655.
- [51] Cassidy, K. J., Gavriely, N., and Grotberg, J. B., 2001, "Liquid plug flow in straight and bifurcating tubes," *J. Biomech. Eng.*, **123**(6), pp. 580–589.
- [52] Crystal, R. G. and J. B. West, 1991, *The lung: scientific foundations*, ed, R. G. Crystal et al., Vol. 1, New York, NY, Raven Press, 2224 see p. 199.
- [53] Serafini, S., and Michaelson, E., 1977, "Length and distribution of cilia in human and canine airways," *Bull. Eur. Physiopathol. Respir.*, **13**, pp. 551–559.
- [54] Davis, S. S., 1973, Rheological examination of sputum and saliva and the effect of drugs, In: *Rheology of Biological Systems*, H. L. Gabelnick and M. Litt, eds, Charles C. Thomas, Springfield, pp. 157–194.
- [55] Sleight, M. A., Blake, J. R., and Liron, N., 1988, "The propulsion of mucus by cilia," *J. Endocrinol.*, **137**, pp. 726–741.